Catalysis Today 149 (2010) 388–393

Contents lists available at ScienceDirect

Catalysis Today

journal homepage: www.elsevier.com/locate/cattod

Perovskite-type oxides in methane dry reforming: Effect of their incorporation into a mesoporous SBA-15 silica-host

Issarly Rivas, Juan Alvarez, Eglé Pietri, M. Josefina Pérez-Zurita, Mireya R. Goldwasser *

Escuela de Química, Centro de Catálisis, Petróleo y Petroquímica, Apartado 40600, Los Chaguaramos, Caracas 1020 A, Venezuela

ARTICLE INFO

Article history:
Available online 28 July 2009

Keywords:
Perovskite-type oxides
Ni-based catalysts
SBA-15 mesoporous silica
Methane dry reforming
Syngas production

ABSTRACT

A series of Ni-based perovskite-type oxides $LaNiO_3$, $La_{0.8}Ca_{0.2}NiO_3$ and $La_{0.8}Ca_{0.2}Ni_{0.6}Co_{0.4}O_3$, were synthesized as catalyst precursors both bulk and built-in a highly ordered mesoporous SBA-15 silica-host with the aim of using them as heterogeneous catalysts in syngas production by the methane dry reforming with CO_2. The solids were characterized by means of FT-IR, XRD, BET surface area and TPR techniques. All synthesized oxides showed a perovskite-type structure. Incorporation of the oxides into the mesoporous silica-host generates a higher metal–support interaction increasing the Ni reduction temperature. A decrease in CH_4 and CO_2 conversion was observed when a second cation in A- and/or B-site was added to the bulk perovskite. The built-in of these solids in the SBA-15 mesoporous silica-host allows working at lower temperature with an increase in conversions and selectivity towards syngas which represent an attractive perspective for industrial application.

1. Introduction

Among all processes to transform methane to syngas, the CO_2 dry reforming of methane produces the lower molar ratio of H_2/CO, suitable to be transformed to more valuable products through various chemical processes such as Fischer Tropsch synthesis and oxo-synthesis. An alternative application of the dry reforming is the thermochemical storage and transmission of renewable energy sources. Specifically, the process Solchem [1] and the CLEA project [2] used the reaction of methane reforming with CO_2 and its reverse methanation reaction as a mean of converting solar energy into chemical energy, which is easier to store and carry. Besides, this reaction consumes CO_2 a greenhouse gas processing it to higher added value products [3–6].

Recently interest has arisen in perovskite-type oxides as precursors in the catalytic dry reforming of CH_4 with CO_2 [7–10]. These solids have high thermal and hydrothermal stability as well as high mechanical strength among other properties. However, the potential application of these oxides is limited by its small surface area, lower than 10 m^2/g [11] and the high reaction temperatures necessary to carry out the reforming due to its endothermicity [9–11].

One way to remedy this problem is to disperse the perovskite-type oxide in a medium that possesses a high specific surface area, thermal stability and prevent the sintering of the metal [12]. Energy consumption in the process of reforming of methane can be significantly reduced by optimizing the design of highly active and selective catalysts; the ordered SBA-15 mesoporous silica meets these features. Applications of ordered mesoporous silica as hosts for the preparation of mesoporous catalysts with chemically functionalized surfaces have been investigated [13–15].

We have previously reported the catalytic performance of a series of binary and ternary Ni-based perovskite-type oxides for dry reforming of methane [9–11,16–18]. Results showed that perovskite systems are good precursors for the dry reforming reaction since, in most cases, they present better catalytic properties quantified in terms of activity, selectivity and stability, comparable even with a catalyst commercially used in steam reforming [9]. The good performance shown by these systems in the reforming reaction has been attributed to the in situ formation of highly dispersed systems (metal particles from B-site cations/A-site cations oxides) as a result of drastic structural changes being experienced by the network of the original crystalline perovskite-type synthesized material after reduction. However, the specific surface area of these catalysts did not meet the requirements needed for industrialization.

The objective of the present work was to investigate the performance of perovskite-type oxides dispersed in an ordered SBA-15 mesoporous silica-host as catalyst precursors for the CO_2 reforming of CH_4 to syngas in order to increase surface area, prevent carbon formation and reduce the high temperatures needed for the reforming reaction lowering energy consumption. $AA'BB'O_3$ ($A = La^{3+}$, $A' = Ca^{2+}$, B = Ni and B′ = Co) perovskite-type oxides were used as catalysts precursors both bulk and built-in a

* Corresponding author. Fax: +58 0212 6051265.
E-mail address: mireya.goldwasser@ciens.ucv.ve (M.R. Goldwasser).

0920-5861/$ – see front matter © 2009 Elsevier B.V. All rights reserved.
doi:10.1016/j.cattod.2009.05.028

SBA-15 mesoporous silica-host. Correlations between the effect of partial substitution of cations in A and/or B sites of the precursor perovskite and the catalytic activity and stability of in situ created Ni and Co nanoparticles in the mesoporous silica-host are discussed.

2. Experimental

2.1. Catalyst synthesis

2.1.1. Synthesis and characterization of SBA-15 mesoporous silica-host

Highly ordered SBA-15 mesoporous silica was synthesized according to the method described by Wang et al. [15]. A typical synthesis procedure is as follows: 12 g of TCP $EO_{20}PO_{70}EO_{20}$ triblock polymer (Aldrich) with a molecular weight of ~5800 g/mol was dissolved in 60 mL of HCl (35–37%) and 350 g of distilled water with stirring at 40 °C for 2 h to make a homogeneous clear solution. Then 29.5 g of the tetraethylorthosilicate (TEOS) was added into that solution and left for 48 h at 40 °C with vigorous stirring to form a solid precipitate, which was filtered and washed with distilled water until pH 7. The solid product was recovered, dried at 50–70 °C for 5 h and calcined at 520 °C for 6 h in air flow.

The SBA-15 mesoporous silica-host was characterized by FT-IR spectroscopy in a Perkin Elmer spectrometer, in the range of 4000–400 cm^{-1}, using potassium bromide (KBr) pellets with a sample/KBR ratio of 1:3. 75 scans were recorded at 20 °C with a resolution of 4 cm^{-1}.

XRD analysis at low angles was used to determine the hexagonal ordering of the mesoporous silica using a diffractometer Bruker Model D8 Advance, using nickel-filtered Cu Kα radiation with λ = 1.5406 Å, in the range of 0.5–5° (2θ).

Samples were characterized by N_2 adsorption/desorption isotherms to obtain the textural properties of the solid at liquid nitrogen temperature in an automated physisorption instrument (Micromeritics Tristar 3300). Prior to the analysis, the samples were outgassed in vacuum at 300 °C overnight.

2.1.2. Synthesis and characterization of perovskite-type catalyst precursors

The studied perovskite-type oxides $LaNiO_3$, $La_{0.8}Ca_{0.2}NiO_3$ and $La_{0.8}Ca_{0.2}Ni_{0.6}Co_{0.4}O_3$ were synthesized by fine chemical using a modification of the citrate sol–gel method investigated first by Pechini, as described elsewhere [9]. Adequate amounts of the precursor of the cation at B-site were dissolved under vigorous stirring in a solution of citric acid (99.5 Riedel-de Haën) with an excess of ethylene glycol (99.5 Riedel-de Haën) as the organic polydentate ligand. The citric acid/B-cation molar ratio was 4, while it was 1.38 for ethylene glycol/citric acid. The mixture was kept at 50–60 °C with mild continuous stirring until a clear solution was obtained. At this point, a stoichiometric quantity of the precursor of A-cation, $La(NO_3)_3{\cdot}5H_2O$, was added while keeping the mixture at 60 °C. The evaporating process proceeded for 2 days until a viscous resin was formed. The resin was dried at 150 °C for 24 h and calcined in air at 700 °C for 5 h.

Perovskite-type oxides loaded into SBA-15 mesoporous silica-host were synthesized by the method described by Yin et al. [12]. Alcoholic solutions of the precursor cations under the nitrate form (La, Ca, Ni and/or Co) were dissolved in the minimum amount of ethanol (solution 1) to obtain the perovskite with a 10% (w/w) Ni in the catalyst. Citric acid was added to solution 1 until a citric acid/cations molar ratio equal to 1 (solution 2). Subsequently, the solution 2 was added to SBA-15 mesoporous silica, left to dry for 24 h and calcined at 600 °C for 6 h in an air flow (30 mL/min). SBA-15 loaded perovskite solids are referred as $LaNiO_3$/SBA-15, $La_{0.8}Ca_{0.2}NiO_3$/SBA-15 and $La_{0.8}Ca_{0.2}Ni_{0.6}Co_{0.4}O_3$/SBA-15.

The crystalline phase detection of the as-synthesized perovskites were determined using a Philips diffractometer model PW 1830 using Cu Kα radiation with λ = 1.5406 Å, between 10° and 80° (2θ) and compared with JCPDS standard files software using the program database PCPDFWIN. Surface areas were measured by a multiple-point BET procedure using nitrogen–argon adsorption at liquid nitrogen temperature with 30% N_2 in Ar in a Micromeritics Tristar 3300 system. The reducibility of these precursor mixed-oxide perovskites was studied by TPR analysis performed in a Thermo-Quest TPD/TPR 1100 system using 0.07 g of the sample in 10% H_2 in Ar stream (20 mL/min). The temperature was raised from room temperature to 1000 °C at a rate of 10 °C/min.

2.2. Activity test

The variation of activity/selectivity patterns as a function of the composition of the mixed-oxide precursors, the influence of activation procedure and reaction parameters were monitored between 600 and 700 °C with a 24 L h^{-1} g^{-1} hourly space velocities using 200 mg of catalyst in a 20-mm i.d. quartz reactor at atmospheric pressure operated in a fixed-bed continuous flow system with feed molar ratio CH_4/CO_2 = 1, using argon as diluents gas with $CH_4/CO_2/Ar$ = 1:1:8, as previously described [9].

The reaction mixture was fed at a total flow rate of 80 mL/min. Before the catalytic tests, the solids were reduced in H_2 flow (20 mL/min, T = 700 °C, 8 h). After reduction, the system was swept with Ar for 15 min and adjusted to reaction temperature. The water produced during reaction, was condensed before passing the reactants and products to the analyzing system, which consisted of an on-line gas chromatograph (Perkin-Elmer Clarus 500) equipped with a TCD detector and provided with a Carbosieve SII 80/100 column (12 ft, 1/8 in. o.d. SS), as previously described [16]. The CH_4 and CO_2 conversions are defined as the CH_4 and CO_2 converted per total amount of CH_4 and CO_2 fed, respectively. The selectivity to CO was calculated based in carbon balance and defined as $S_{CO}\,(\%) = \eta_{CO}/[\eta_{CH_4(c)} + \eta_{CO_2(c)}] \times 100$; while hydrogen selectivity was calculated as $S_{H_2}\,(\%) = [\eta_{H_2}/2\eta_{CH_4(c)}] \times 100$, where η_{CO} and η_{H_2} are the moles of CO and hydrogen produced and $\eta_{CH_4(c)}$ and $\eta_{CO_2(c)}$ are the amounts of methane and carbon dioxide converted, as described elsewhere [17]. Stability tests were performed at 700 °C for 24 h.

3. Results and discussion

3.1. FT-IR and XRD analysis of SBA-15 mesoporous silica

Evidence of SBA-15 mesoporous silica synthesis was followed by FT-IR and low angle XRD analysis. Fig. 1 shows the FT-IR spectrum of SBA-15 mesoporous silica. Characteristic bands are

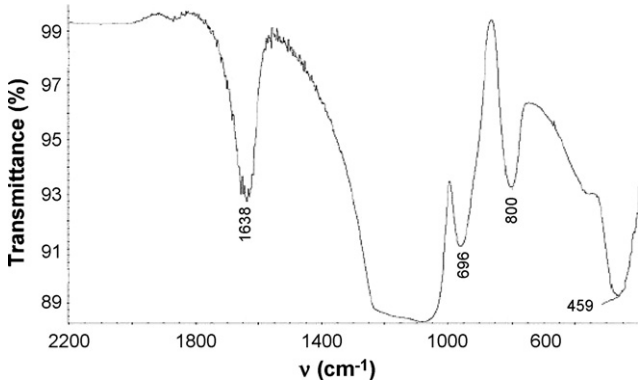

Fig. 1. FT-IR spectrum of SBA-15 mesoporous silica-host.

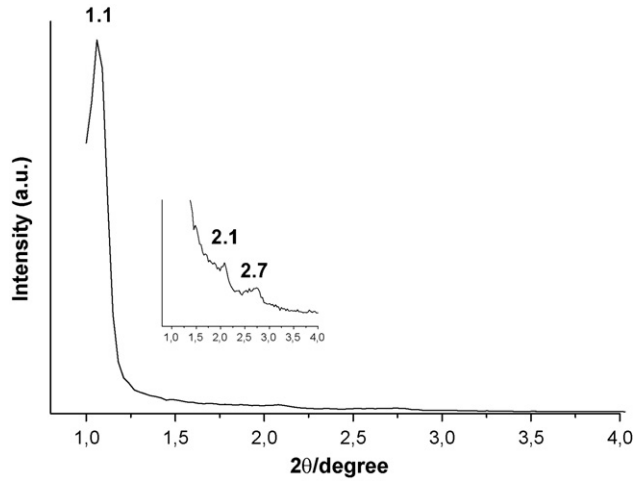

Fig. 2. XRD pattern of SBA-15 mesoporous silica-host at low angles.

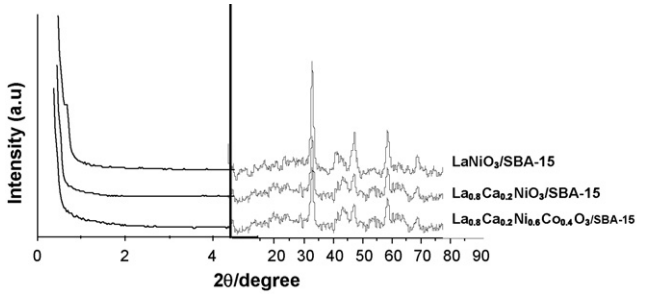

Fig. 3. XRD patterns of perovskite-type oxides loaded into the SBA-15 mesoporous silica-host at low and high angles.

observed at 466, 807, 960 and 1085 cm^{-1} corresponding to vibrations of Si–O–Si bonds. The band at 466 cm^{-1} is attributed to rocking vibrations, the 807 cm^{-1} band for bending and at 1085 cm^{-1} due to stretching vibrations of these bonds. The 960 cm^{-1} band is assigned to Si–OH silanols groups present in the mesoporous structure. Additionally, a band around 1630 cm^{-1} due to the presence of TCP hydroxyl groups (–OH) was observed [19].

XRD pattern of SBA-15 mesoporous silica at low angles is shown in Fig. 2. Three diffraction peaks are present: a very intense one at $2\theta = 1.1^\circ$ and two weak peaks at $2\theta = 2.1^\circ$ and $2\theta = 2.7^\circ$ respectively, corresponding to a hexagonal arrangement characteristic of this type of mesoporous solids [20,21], confirming formation of the highly ordered mesoporous structure.

Fig. 3 shows the XRD patterns of perovskite-type oxides loaded into the SBA-15 mesoporous silica-host at low and high angles. It is observed that as Ni^{3+} and/or La^{3+} are partially substituted by Co^{3+} and/or Ca^{2+}, the intensity of the perovskite peaks decrease. For $LaNiO_3$/SBA-15 a decrease in the intensity of the diffraction peaks of the hexagonal arrangement and shifting to higher angles is observed. This could be due to both confinement of the perovskite-type oxide within the mesoporous channels of SBA-15 structure and to the dilution effect brought about by adding the perovskite phase [22,23]. In addition, the partial substitution of cations in A- and B-sites for $La_{0.8}Ca_{0.2}NiO_3$ and $La_{0.8}Ca_{0.2}Ni_{0.6}Co_{0.4}O_3$ loaded in the silica-host, produced a distortion of the pores of the mesoporous structure, since the peaks characteristic of the hexagonal structure are not observed.

XRD patterns at higher angles of as-synthesized and after calcined perovskites type oxides both bulk and loaded into the SBA-15 mesoporous silica-host are shown in Fig. 4. Main peaks characteristic of ABO_3 perovskite structure are clearly shown. A decrease in the intensity of the peaks of the perovskite built-in the mesoporous silica-host was observed due to the confinement of the oxide in the mesoporous channels.

3.2. Textural characterization

The textural characteristics of the support and catalysts have been evaluated from the corresponding N_2 adsorption/desorption isotherms. Table 1 summarizes the textural properties of the solids.

Fig. 5 presents the isotherms of SBA-15 mesoporous silica-host; a typical type *IV* isotherm is observed showing the hysteresis loop characteristic of mesoporous solids. The observed inflection in the region $P/P_o \sim 0.5$ is usually attributed to the presence of tubular-shaped capillaries opening at both ends. Similarly, an increase in the N_2 adsorbed volume at $P/P_o < 0.3$ is associated with the presence of microporosity in the solid [24]. The mesoporous size distribution obtained by the BJH method resulted very narrow for this solid, as shown in the insert of Fig. 5.

Incorporation of the perovskite-type oxide, inside the mesoporous channels of the SBA-15 silica-host generates a distortion of the mesoporous shape and changes in the shape of the isotherms are observed; the hysteresis loop being clearly present only for $LaNiO_3$/SBA-15. For $La_{0.8}Ca_{0.2}NiO_3$/SBA-15 and $La_{0.8}Ca_{0.2}Ni_{0.6}Co_{0.4}O_3$/SBA-15, the adsorption–desorption isotherms did not show the typical features of the mesoporous; however, a slight hysteresis was observed at high N_2 relative pressure, being closer to that of macroporous solids (Fig. 6). Moreover, the important raise of the amount of N_2 adsorbed in the range of relative pressures < 0.3 was not observed. This fact could be explained by the partial blocking of the porous network by the presence of large perovskite-type crystallites. The most important changes observed when loading the perovskite-type oxides inside the mesoporous channels of the SBA-15 silica-host could be attributed to: (i)

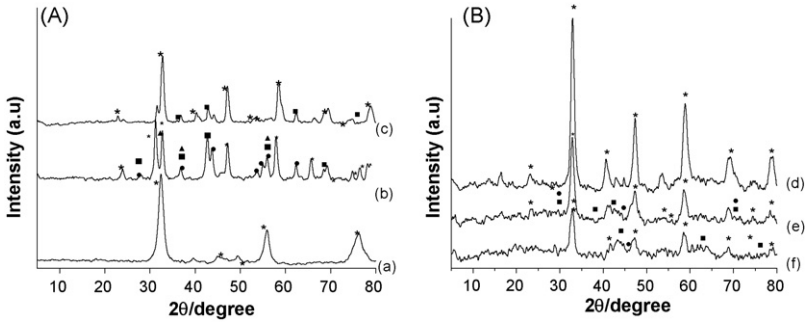

Fig. 4. XRD patterns at higher angles of as-synthesized and after calcined perovskite-type oxides: (A) bulk and (B) built-in SBA-15 mesoporous silica-host. (a) $LaNiO_3$; (b) $La_{0.8}Ca_{0.2}NiO_3$; (c) $La_{0.8}Ca_{0.2}Ni_{0.6}Co_{0.4}O_3$; (d) $LaNiO_3$/SBA-15; (e) $La_{0.8}Ca_{0.2}NiO_3$/SBA-15; (f) $La_{0.8}Ca_{0.2}Ni_{0.6}Co_{0.4}O_3$. Phases: (*) $LaNiO_3$; (■) NiO; (●) La_2O_3; (▲) CaO.

Table 1
Textural properties of as-synthesized solids.

Catalyst precursor	BET surface area (m^2/g)	External surface area (m^2/g)	Microporous area (m^2/g)	Pore volume (cm^3/g)	Microporous volume (cm^3/g)	Pore diameter (nm)
SBA-15	620	246	374	0.58	0.11	4.0
$LaNiO_3$/SBA-15	81	70	11	0.18	0.01	8.6
$La_{0.8}Ca_{0.2}NiO_3$/SBA-15	65	51	14	0.16	0.01	12.5
$La_{0.8}Ca_{0.2}Ni_{0.6}Co_{0.4}O_3$/SBA-15	23	22	1	0.15	–	26

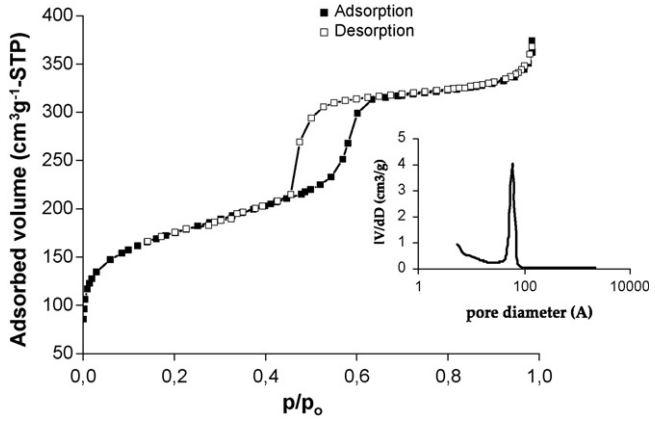

Fig. 5. Adsorption/desorption isotherm and pore size distribution of SBA-15 mesoporous silica-host.

decrease of the internal and external surface area, (ii) increase of the pore diameter and (iii) decrease of the pore volume.

The first two observations are a consequence of the incorporation of the oxide into the silica-host channels which leads to a distortion of the mesoporous shape, increasing its size. A decrease of pore volume (iii) is usually a consequence of obstruction of the mesoporous of the silica-host by the crystallites of the perovskite-type oxide when loaded. However, partial sintering of the SBA-15 mesoporous silica during the thermolysis process to originate the hosted perovskite is not discarded. As suggested by Valange et al. [25], the whole system can be considered as almost completely mesoporous with numerous interconnections, which is in agreement with the observed increase in pore diameter shown in Table 1. Further work has to be carried out in order to reach a more concise explanation.

The observed results are in agreement with those seen by XRD analysis of the loaded perovskites-type oxides at low angles (Fig. 2), showing that the intensity of the diffraction peaks of the hexagonal structure decreased. A similar result has been reported by Albuquerque et al., for CaO supported on mesoporous silica [21].

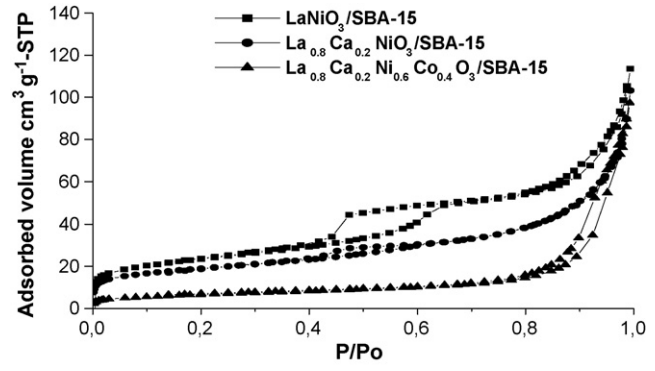

Fig. 6. Adsorption/desorption isotherm of perovskite-type oxides incorporated into SBA-15 mesoporous silica-host.

3.3. TPR studies

Fig. 7 shows the TPR profiles of perovskite-type oxides: (A) bulk and (B) loaded into a SBA-15 mesoporous silica-host. Analysis of the reduction profiles for all samples showed formation of several peaks, corresponding to different Ni and/or Co intermediate species through a two-step mechanism in which the Ni^{3+} and Co^{3+} are reduced to Ni^{2+} and Co^{2+} followed by reduction to Ni^0 and Co^0.

During the reduction of $LaNiO_3$ (Fig. 7A, a); a signal at 325 °C indicates formation $LaNiO_{2.75}$ without total destruction of the perovskite-type structure [11]. The second peak at 484 °C corresponds to $La_2Ni_2O_5$ phase, and the third at 540 °C reducing to Ni^0 and La_2O_3. Based on these results, the main reduction steps could be written as follows:

$$LaNiO_3 + 0.25H_2 \rightarrow LaNiO_{2.75} + 0.25H_2O \quad (1)$$

$$4LaNiO_{2.75} + H_2 \rightarrow La_4Ni_3O_{10} + Ni^0 + H_2O \quad (2)$$

$$La_4Ni_3O_{10} + 4H_2 \rightarrow 2La_2O_3 + 3Ni + 4H_2O \quad (3)$$

When $LaNiO_3$ perovskite-type oxide is hosted in the mesoporous silica (Fig. 7B, d) a new peak at 348 °C is observed corresponding to nickel oxide (NiO) from the Ni precursor salt during synthesis which was not forming part of the perovskite structure. This reduction peak is generally observed at temperatures between 200 and 270 °C. The other two maxima at 414 and 622 °C, corresponding to the reduction of Ni^{3+} to Ni^{2+} and Ni^{2+} to Ni^0 respectively, follow a reduction scheme similar to that proposed for the bulk perovskite. However, the fact that the reduction of the perovskite occurs at higher temperatures (maxima at 414 and 622 °C) and the broadening of the signal, indicate a strong interaction between the Ni from the perovskite and the SBA-15 mesoporous silica-host.

TPR profile of $La_{0.8}Ca_{0.2}NiO_3$, both bulk (Fig. 7A, b) and loaded into the SBA-15 silica-host (Fig. 7B, e) shows that the partial substitution of La^{3+} by Ca^{2+} in the perovskite structure assists the process of reduction, compared to that of $LaNiO_3$ perovskite, as confirmed by the shifting of the temperature of the reduction maxima to lower values (411 and 570 °C). This effect can be attributed to the replacement of La^{3+} by Ca^{2+} (smaller charge and ionic radius than La^{3+}), which generates instability to the perovskite structure, increasing the mobility of oxygen in the system and facilitating their elimination as water during the reduction process. In order to maintain certain stability, the structure could change the Ni ions oxidation states to higher values or form an oxygen deficient perovskite structure such as $La_{0.8}Ca_{0.2}NiO_{3-\delta}$. In both cases the resulting structure is more easily reducible. This effect has been previously reported by our group for bulk perovskite-type oxides [9,10,26].

Similarly, the presence of Ca^{2+} in the perovskite seems to reduce the Ni–SBA-15 interaction since for $La_{0.8}Ca_{0.2}NiO_3$/SBA-15 reduction signals appeared at lower temperatures.

TPR profile of $La_{0.8}Ca_{0.2}Ni_{0.6}Co_{0.4}O_3$ bulk (Fig. 7A, b) shows two reduction signals at 443 and 600 °C. As before, these signals are due to a two-step reduction of the perovskite structure corresponding to Ni^{3+} to Ni^{2+} (first step) and the reduction of these last species to

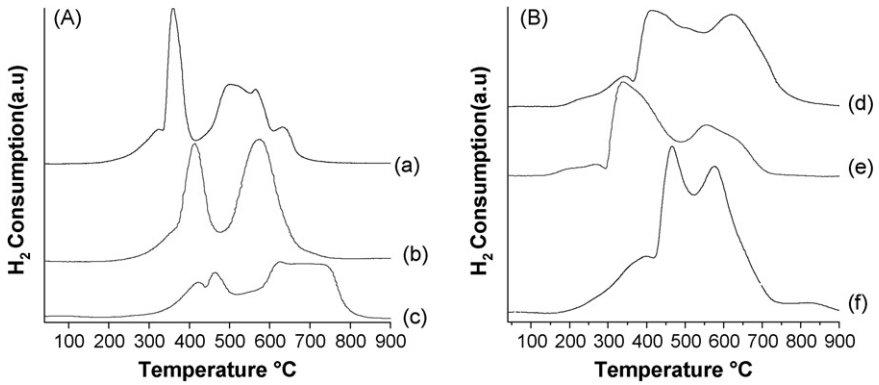

Fig. 7. TPR profiles of perovskite-type oxides: (A) bulk and (B) built-in SBA-15 mesoporous silica. (a) $LaNiO_3$; (b) $La_{0.8}Ca_{0.2}NiO_3$; (c) $La_{0.8}Ca_{0.2}Ni_{0.6}Co_{0.4}O_3$; (d) $LaNiO_3$/SBA-15; (e) $La_{0.8}Ca_{0.2}NiO_3$/SBA-15; (f) $La_{0.8}Ca_{0.2}Ni_{0.6}Co_{0.4}O_3$/SBA-15.

Ni^0 (second step). However, as we have previously reported [26] Co^{3+} species present in the perovskite oxide can simultaneously be reduced to Co^{2+} at that temperature. An overlap in the profile is observed for peaks maxima at 579 and 659 °C which could correspond to the reduction of Ni^{2+} to Ni^0 and Co^{2+} to Co^0. The reduction temperatures achieved for this precursor reveal a possible Co–Ni metal interaction, since these temperatures are between those recorded in previous work for $LaCoO_3$ and $LaNiO_3$ precursors [11].

Finally, the small maximum observed at higher temperature (724 °C) is attributed to Ni^{2+} ions and/or Co^{2+} occupying positions inside the channels of the mesoporous solid which difficult its reduction.

For $La_{0.8}Ca_{0.2}Ni_{0.6}Co_{0.4}O_3$/SBA-15 a strong interaction seems to exist between the perovskite and the mesoporous silica-host resulting in a poorly defined reduction profiles. Formation of a single (or even multilayer) Ni^{2+} (or Co^{2+}) silicate along the calcined step is not discarded. Suh et al. [27] reported that formation of nickel silicate on the catalyst increases the total surface area of the catalysts, and reduces the nickel particle size as well as its reducibility. Nickel silicate also makes the silica surface rough, thus reducing the pore opening of the support. Similarly, we have found this type of interaction when working with Co/HMS [28].

3.4. Activity results

Catalytic results obtained in the dry reforming of CH_4 with CO_2 after 24 h on stream are shown in Table 2. Values for the CH_4 and CO_2 conversion, H_2 produced by CH_4 converted and H_2/CO experimental product ratios are shown. Under the used experimental conditions, all the catalyst systems were active for the studied reaction, with CH_4 conversions above 55%. Similarly, steady-state conditions for these systems were rapidly reached, remaining constant for up to 24 h on stream as shown in Fig. 8.

On $LaNiO_3$ bulk perovskite (Table 2) conversions of CH_4 and CO_2 are quite similar indicating that the main occurring reaction is the dry reforming reaction, also confirmed by the fact that the molar H_2/CO ratio is ~1.

When La^{3+} was partially replaced by Ca^{2+} in the bulk perovskite to form $La_{0.8}Ca_{0.2}NiO_3$ to inhibit coke formation due to Ca^{2+} basic character, CH_4 and CO_2 conversions decrease as compared to those obtained over $LaNiO_3$ bulk perovskite, and the CH_4/CO_2 molar ratio was lower than the expected stoichiometric ratio of 1 (Table 2). This difference in conversion indicates the presence of side reactions such as the reverse water-gas shift reaction (4), which is favoured at high temperature. The influence of this reaction is reflected in a higher conversion of CO_2 over CH_4 and in a H_2/CO molar ratio lower than 1.

$$CO_2 + H_2 \rightarrow CO + H_2O, \quad \Delta H^{\circ}_{25\,^{\circ}C} = 41\ \text{kJ/mol} \tag{4}$$

The lower activity shown by $La_{0.8}Ca_{0.2}NiO_3$ bulk perovskite (55% CH_4 conversion) compared to that of $LaNiO_3$ bulk perovskite (85% CH_4 conversion, Fig. 8) seems to be due to the substitution of La^{3+} by a cation of lower ionic radium (Ca^{2+}) which decreases the stability of the perovskite structure requiring a charge compensation, giving rise to the existence of unusual cationic valence states. We have previously observed a similar effect for $La_{0.8}Ca_{0.2}Ru_{0.8}Ni_{0.2}O_3$ [10]. In addition, segregation of Ca with the subsequent decrease in the number of exposed Ni sites could also be taking place.

When both A- and B-site cations are simultaneously replaced to form $La_{0.8}Ca_{0.2}Ni_{0.6}Co_{0.4}O_3$ bulk perovskite-type oxide a similar effect occurs, but the presence of Co, which assists the Ni reduction, makes the decrease on activity (66%) less marked than for $La_{0.8}Ca_{0.2}NiO_3$ bulk perovskite [26]. Again the occurrence of the reverse water-gas shift reaction is noted giving rise to higher CO_2 conversions and H_2/CO molar ratio lower than 1.

Table 2
Catalytic results of perovskite-type oxides bulk and built-in a SBA-15 mesoporous silica.

Catalyst precursor	X_{CH_4} (%)	X_{CO_2} (%)	H_2/CO (molar ratios)	$H_2/CH_{4(c)}$ (molar ratios)
$LaNiO_3$ [a]	85	87	0.90	1.90
$La_{0.8}Ca_{0.2}NiO_3$ [a]	55	71	0.80	1.30
$La_{0.8}Ca_{0.2}Ni_{0.6}Co_{0.4}O_3$ [a]	66	80	0.80	1.40
$LaNiO_3$/SBA-15[a]	88	91	0.90	1.90
$La_{0.8}Ca_{0.2}NiO_3$/SBA-15[a]	82	88	1.00	2.00
$La_{0.8}Ca_{0.2}Ni_{0.6}Co_{0.4}O_3$/SBA-15[a]	86	88	1.00	1.90
$LaNiO_3$/SBA-15[b]	63	74	0.87	1.54
$La_{0.8}Ca_{0.2}NiO_3$/SBA-15[b]	69	70	1.04	2.00
$La_{0.8}Ca_{0.2}Ni_{0.6}Co_{0.4}O_3$/SBA-15[b]	53	65	0.84	1.70

[a] $T_{reaction}$ = 700 °C.
[b] $T_{reaction}$ = 600 °C; CH_4:CO_2:Ar = 1:1:8; VE = 24 L h^{-1} g^{-1}; m_{cat} = 200 mg, P = 1 atm, time = 24 h.

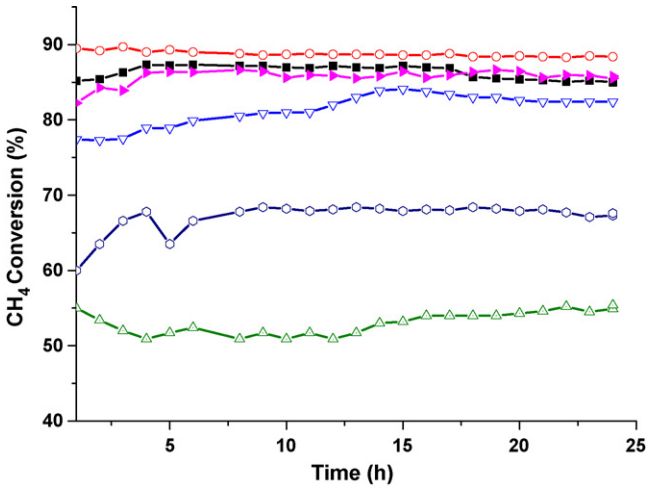

Fig. 8. Stability test in the dry reforming of methane on perovskite-type oxides bulk and built-in a SBA-15 mesoporous silica: CH_4:CO_2:Ar = 1:1:8; GHSV = 24 L h^{-1} g^{-1}, W_{cat} = 0.2 g, P = 1 atm, T_{red} = 600 °C/4 h. $T_{reaction}$ = 700 °C/4 h. (■) $LaNiO_3$; (○) $LaNiO_3$/SBA-15; (△) $La_{0.8}Ca_{0.2}NiO_3$; (▽) $La_{0.8}Ca_{0.2}NiO_3$/SBA-15; (⬡) $La_{0.8}Ca_{0.2}Co_{0.4}Ni_{0.6}O_3$; (►) $La_{0.8}Ca_{0.2}Co_{0.4}Ni_{0.6}O_3$/SBA-15.

When the perovskites-type oxides are built-in the silica-host increase of both, CH_4 and CO_2 conversion is produced as compared to the bulk perovskite (Table 2 and Fig. 8). In all cases the H_2/CO molar ratio was close to 1, indicating that only the reforming reaction is taking place. In accordance, the molar ratio of H_2 produced/CH_4 converted follows the expected stoichiometric value of 2. On $La_{0.8}Ca_{0.2}NiO_3$/SBA-15, the increase in CH_4 and CO_2 conversion was more significant. The stability of all SBA-15 hosted perovskites was excellent, no decrease in the CH_4 conversion was observed after continuous reaction at 700 °C for 24 h and the observed smoothness of the experimental points indicating that the SBA-15 silica helped the heat transfer of the highly endothermic reforming reaction avoiding both, formation of cold points on the solids and sintering of Ni–Co crystallites during reaction.

Aiming to lower energy consumption, tests were conducted over the perovskite oxides loaded into the silica-host at a lower reaction temperature. As observed in Table 2, even at temperature as low as 600 °C, high CH_4 and CO_2 conversions were obtained.

Results show that at 600 °C on $La_{0.8}Ca_{0.2}NiO_3$/SBA-15, the main reaction taking place is the CO_2 reforming of CH_4, while on $LaNiO_3$/SBA-15 and $La_{0.8}Ca_{0.2}Ni_{0.6}Co_{0.4}O_3$/SBA-15 the reverse water-gas shift reaction takes place together with the reforming reaction resulting in a slightly higher CO_2 conversion compare to CH_4 and a H_2/CO molar ratio lower than 1.

The observed improvement of the catalytic performance of the perovskite-type materials when they are built-in the highly ordered mesoporous SBA-15 silica-host could be explained in two ways: (i) higher dispersion of the perovskite-type oxides are obtained when incorporated into the SBA-15 mesoporous silica and (ii) there is a dilution effect exerted by the mesoporous material which minimize the heat diffusion problems related to this highly endothermic reaction.

4. Conclusions

The XRD analysis indicates that incorporation of the perovskite-type oxide into the mesoporous silica-host produces a distortion of the pores decreasing the channel hexagonal arrangement characteristic of the SBA-15 mesoporous silica. A decrease in the intensity of the peaks characteristic of the ABO_3 structure was produced due to confinement of the oxide in the silica-host channels.

Partial substitution of A and/or B cations of loaded perovskite produces deformation of the mesoporous structure of the ordered silica which evolve to a macroporous structure. However, the incorporation of these solids in the SBA-15 mesoporous silica-host gives rise to well dispersed nano-metallic (Ni–Co) particles inside the mesoporous of SBA-15 silica-host by decomposition and further reduction of the built-in perovskite.

TPR analysis showed a strong interaction between the perovskite oxide and the SBA-15 silica-host, which causes an increase in the temperature of reduction as compared to the bulk perovskite.

Partial substitution of A- and/or B-site cations of the perovskite produces a decrease in the conversion of CH_4 and CO_2. However, the incorporation of these solids in the SBA-15 mesoporous silica-host exerts a positive effect on the activity/selectivity of the reaction since it allows an increase in the conversion of CH_4 and CO_2 and the molar H_2/CO and allows working at lower temperature which represents an attractive perspective for industrial application.

Acknowledgments

The authors are grateful for financial support from the Council of Scientific and Humanistic Development of Venezuelan Central University (UCV-CDCH) and the Draft Law on Science and Technology (LOCTI), through projects PG-03-00-6504-2006 and LOCTI-2007-2008, respectively.

References

[1] T. Hayakawa, A.G. Andersen, M. Shimizu, K. Suzuki, K. Takehira, Catal. Lett. 22 (4) (2004) 307.
[2] L.A. Marschall, G.A. Snyder, J.J. Sudol, C. Toner, P.R. Cooper, American Astronomical Society Meeting 207, #66.03, Bull. Am. Astronom. Soc. 37 (2005) 1261.
[3] J.H. Lunsford, Catal. Today 63 (2000) 165–174.
[4] C.B. Dupeyrat, G.A. Sierra, F. Mondragón, J. Barrault, J.M. Tatibouét, Catal. Today 107–108 (2005) 474–480.
[5] H.W. Chen, C.Y. Wang, C.H. Yu, L.T. Tseng, P.H. Liao, Catal. Today 97 (2004) 173–180.
[6] J. Rynkoswski, P. Samulkiewicz, A.K. Ladavos, P.J. Pomonis, Appl. Catal. A: Gen. 263 (2004) 1–9.
[7] J. Guo, H. Lou, H. Zhao, D. Chai, X. Zheng, Appl. Catal. A: Gen. 273 (2004) 75–82.
[8] J.B. Wang, Y.S. Wu, T.J. Huang, Appl. Catal. A: Gen. 272 (2004) 289–298.
[9] M.R. Goldwasser, M.E. Rivas, E. Pietri, M.J. Pérez-Zurita, M.L. Cubeiro, L. Gingembre, L. Leclercq, G. Leclercq, Appl. Catal. A: Gen. 255 (2003) 45–57.
[10] M.R. Goldwasser, M.E. Rivas, E. Pietri, M.J. Pérez-Zurita, M.L. Cubeiro, A. Grivobal-Constant, G. Leclerq, J. Mol. Catal. A: Chem. 228 (2005) 325–331.
[11] G. Valderrama, A. Kiennemann, M.R. Goldwasser, Catal. Today 133–135 (2008) 142–148.
[12] N. Yin, Y. Cao, Y. Su, W.L. Dai, H.Y. He, K.N. Fan, J. Catal. 230 (2005) 249–253.
[13] X. Chen, H. Hu, B. Liu, M. Qiao, K. Fan, H. He, J. Catal. 220 (2003) 254–257.
[14] L. Vradman, M.V. Landau, M. Herskowitz, V. Ezersky, M. Talianker, S. Nikitenko, Y. Koltypin, A. Gedanken, J. Catal. 213 (2003) 163–175.
[15] Y. Wang, M. Noguchi, Y. Takahashi, Y. Ohtsuka, Catal. Today 68 (2001) 3–9.
[16] M.R. Goldwasser, M.E. Rivas, M.L. Lugo, E. Pietri, J. Pérez-Zurita, M.L. Cubeiro, A. Griboval-Constant, G. Leclercq, Catal. Today 107–108 (2005) 106–113.
[17] G. Valderrama, M.R. Goldwasser, C. Urbina de Navarro, J.M. Tatibouet, J. Barrault, C. Batiot-Dupeyrat, F. Martınez, Catal. Today 107–108 (2005) 785–791.
[18] M.E. Rivas, J.L.G. Fierro, M.R. Goldwasser, E. Pietri, M.J. Pérez-Zurita, A. Griboval-Constant, G. Leclercq, Appl. Catal. A: Gen. 344 (2008) 10–19.
[19] G. Eimer, S. Cassuscelli, G. Ghione, M. Crivello, E. Herrero, Appl. Catal A: Gen. 298 (2006) 232.
[20] Q. Wei, H. Chen, Z. Nie, Y. Hao, Y. Wang, Q. Li, J. Zou, Mater. Lett. 61 (2007) 1469–1473.
[21] M. Albuquerque, I. Jiménez, J. Santamaría, J.M. Mérida, R. Moreno, E. Rodríguez, A. Jiménez, D. Azevedo, C. Cavalcante, P. Maireles, Appl. Catal. A: Gen. 334 (2008) 35–43.
[22] S. Nguyen, V. Szabo, D. Trong On, S. Kaliaguine, Micropor. Mesopor. Mater. 54 (2002) 51–61.
[23] A. Martínez, C. López, F. Márquez, I. Díaz, J. Catal. 220 (2003) 486–499.
[24] N. Arellano, M.J. Pérez-Zurita, V. Sazo, C. Urbina de Navarro, C.M. López, Ciencia 16 (2) (2008) 224–232.
[25] S. Valange, R. Palacio, A. Charmot, J. Barrault, A. Louati, Z. Gabelica, J. Mol. Catal. A: Chem. 305 (2009) 24–33.
[26] O. González, J. Lujano, E. Pietri, M.R. Goldwasser, Catal. Today 107–108 (2005) 436–443.
[27] D.J. Suh, J.S. Chung, T. Lim, S.H. Moon, J. Korean Inst. Chem. Eng. 27 (5) (1989) 620–628.
[28] E. Lira, C.M. Lopez, F. Oropeza, M. Bartolini, J. Alvarez, M.R. Goldwasser, F. Lopez Linares, J.-F. Lamonier, M.J. Pérez-Zurita, J. Mol. Catal. A: Chem. 281 (2008) 146–153.